Photodynamic therapy-triggered on-demand drug release from ROS-responsive core-cross-linked micelles toward synergistic anti-cancer treatment

Li, Yongjuan; Hu, Jian; Liu, Xun; Liu, Yong; Lv, Shixian; Dang, Juanjuan; Ji, Yong; He, Jinlin; Yin, Lichen

Published in:
Nano Research

DOI:
10.1007/s12274-019-2330-y

Publication date:
2019

Nano Research
2019, 12(5): 999–1008

ISSN 1998-0124 CN 11-5974/O4
https://doi.org/10.1007/s12274-019-2330-y

Research Article

Photodynamic therapy-triggered on-demand drug release from ROS-responsive core-cross-linked micelles toward synergistic anti-cancer treatment

Yongjuan Li[1], Jian Hu[2], Xun Liu[1], Yong Liu[3] (✉), Shixian Lv[1], Juanjuan Dang[1], Yong Ji[4] (✉), Jinlin He[2], and Lichen Yin[1] (✉)

[1] *Institute of Functional Nano and Soft Materials (FUNSOM), Jiangsu Key Laboratory for Carbon-Based Functional Materials and Devices, Soochow University, Suzhou 215123, China*
[2] *College of Chemistry, Chemical Engineering and Materials Science, Suzhou Key Laboratory of Macromolecular Design and Precision Synthesis, Jiangsu Key Laboratory of Advanced Functional Polymer Design and Application, Soochow University, Suzhou 215123, China*
[3] *Department of Biomedical Engineering, University of Groningen and University Medical Center Groningen, Antonius Deusinglaan 1, 9713 AV Groningen, The Netherlands*
[4] *Department of Cardiothoracic Surgery, Wuxi People's Hospital Affiliated to Nanjing Medical University, Wuxi 214023, China*

Received: 16 December 2018/ **Revised:** 3 February 2019 / **Accepted:** 4 February 2019

ABSTRACT

Polymeric micelles have demonstrated wide utility for chemodrug delivery, which however, still suffer from shortcomings such as undesired drug loading, disassembly upon dilution, pre-leakage of drug cargoes during systemic circulation, and lack of cancer-selective drug release. Herein, a poly(ethylene glycol) (PEG)-polyphosphoester-based, reactive oxygen species (ROS)-responsive, core-cross-linked (CCL) micellar system was developed to encapsulate both chemodrug (doxorubicin, Dox) and photosensitizer (chlorin e6, Ce6). The hydrophobic core of the micelles was cross-linked via a thioketal (TK)-containing linker, which notably enhanced the drug loading and micelle stability. In tumor cells, far-red light irradiation of Ce6 generated ROS to cleave the TK linkers and disrupt the micelle cores. As such, micelles were destabilized and Dox release was promoted, which thereafter imparted synergistic anti-cancer effect with ROS-mediated photodynamic therapy. This study provides an effective approach to realize the precise control over drug loading, formulation stability, and cancer-selective drug release using polymeric micelles, and would render promising utilities for the programmed anti-cancer combination therapy.

KEYWORDS

core-cross-linked micelles, on-demand drug release, photodynamic therapy, reactive oxygen species (ROS) responsiveness, synergistic anti-cancer therapy

1 Introduction

Polymeric micelles (PMs) have been extensively used for anticancer therapeutic delivery, owing to their desired capabilities to enhance the solubility of drugs, prolong blood circulation, improve tumor accumulation through the enhanced permeability and retention (EPR) effect, and reduce side effects [1–5]. Nevertheless, clinical applications of PMs are largely limited by the premature disintegration before they reach the tumor sites [6–8]. Additionally, most of the therapeutics are loaded in PMs via weak hydrophobic interactions, and increasing evidence has suggested that the thermo-dynamic PMs could disassemble in the blood circulation because of the extensive dilution, and the unexpected drug leakage will occur to cause serious side effects [9–11]. Lam et al. found that when the drug loading of micelles was lower than 5 wt.%, polymers inside the micelles were mostly inter-molecularly overlapped [12]. Thereby the micelles possessed suitable and stable sizes to reach the tumor sites through the EPR effect. However, when the drug loading was higher than 5 wt.%, the micelles may re-assemble into bigger micelles with a small portion of drugs (< 19%) leaking from the micelles during the re-assembly [13]. Therefore, it is highly demanded to stabilize the micelle systems while maintaining satisfactory drug loading.

To increase the stability of PMs and prevent the immature drug release, the core-cross-linking strategy has been proposed [14–17]. The chemical cross-linking could effectively resist the dilution-induced micelle disassembly, and the more compact hydrophobic core would afford better drug encapsulation capability. To further enable on-demand drug release in cancer tissues/cells, stimuli-responsive core-cross-linked (CCL) micelles that can undergo selective de-cross-linking upon cancer-specific triggers have been investigated for drug delivery. Commonly utilized stimuli include pH [18, 19], redox [20], reactive oxygen species (ROS) [21, 22], and enzymes [23], etc. However, these triggers often lack cancer selectivity (such as pH and redox), have heterogeneous intensity among different tumor types, or are not strong enough to provoke pronounced responsiveness from the vehicles. For instance, the ROS concentration in cancer cells is often insufficient to trigger the transformation of ROS-responsive domains, such as thioketal (TK) [24], arylboronic acid [25], thioether [26], selenium [27, 28], and tellurium [29, 30]. While development of CCL micelles with higher ROS sensitivity would be a promising approach, it is chemically challenging to design new and ultra-ROS-responsive domain. An alternative approach to

Address correspondence to Lichen Yin, lcyin@suda.edu.cn; Yong Liu, y.liu@umcg.nl; Yong Ji, jiyongmyp@163.com

address this issue could be manually elevating the ROS levels in cancer cells [31, 32], thus magnifying the response of nanovehicles to ROS.

Photodynamic therapy (PDT), involving the production of various types of ROS by photosensitizers (PSs) under light activation, is regarded as a promising strategy for cancer therapy [33–37]. Compared with surgery and chemotherapy, PDT features less invasiveness, better tumor localization, and minimal drug resistance [38–40]. More importantly, the high levels of ROS generated by PDT can not only induce cancer cell apoptosis and necrosis, but can also create a specific ROS-rich microenvironment to trigger on-demand de-cross-linking of the ROS-responsive CCL micelles to enable selective chemodrug release in cancer cells.

Herein, we report the design of a core-cross-linked, poly(ethylene glycol) (PEG)-polyphosphoester-based micellar system for the co-delivery of chemodrug (doxorubicin, Dox) and photosensitizer (chlorin e6, Ce6). The core of the micelles was stabilized via cross-linking by the TK-containing linkers, and the PEG shell could stabilize the whole micellar system and enable long circulation in the blood. Dox and Ce6 were co-encapsulated into the cross-linked hydrophobic core of the CCL micelles, thus preventing premature leakage during systemic circulation. Upon reaching the tumor tissues, the site-specific far red light irradiation (660 nm, 5 mW/cm^2) could generate extensive ROS which can break down the TK cross-linker to destabilize the micelles and trigger instantaneous Dox release. Synergistically, the released Dox and the generated ROS will lead to apoptosis and necrosis of the cancer cells (Scheme 1).

2 Experimental

2.1 Materials, cells, and animals

Ce6 was purchased from Frontier Scientific (Newark, USA). 3-Mercaptopropionic acid, 2-chloroethylamine hydrochloride, o-benzotriazole-N,N,N',N'-tetramethyluronium hexafluorophosphate (HBTU), 1-hydroxybenzotriazole (HOBt), copper(II) sulfate ($CuSO_4$), sodium ascorbate, pentamethyldiethylenetriamine (PMDEM), poly(ethylene glycol) methyl ether (PEG-OH) (M_n = 5 kDa), and sodium azide were purchased from Energy Chemical (Shanghai, China). Dichloromethane (DCM), anhydrous sodium sulfate (Na_2SO_4), anhydrous tetrahydrofuran (THF), diethyl ether (Et_2O), dimethylformamide (DMF), anhydrous acetone, hydrogen peroxide (H_2O_2), and pyrene were purchased from Sinopharm Chemical Reagent Co., Ltd (Shanghai, China). Dox, deuterated chloroform ($CDCl_3$), deuterated water (D_2O), deuterated dichlorosulfoxide (DMSO-d_6), and stannous octoate ($Sn(Oct)_2$) were purchased from J&K (Shanghai, China). All chemicals were used as received unless otherwise indicated. 2-(But-3-yn-1-yloxy)-2-oxo-1,3,2-dioxaphospholane (BYP) was synthesized as reported before [41]. 3-(4,5-Dimethylthiahiazol-2-yl)-2,5-diphenyl-2H-tetrazolium bromide (MTT) was purchased from Invitrogen (Carlsbad, CA, USA).

4T1 (mouse mammary carcinoma) and MCF-7 (human breast adenocarcinoma) cells were purchased from the American Type Culture Collection (Rockville, MD, USA). MCF-7 cells were cultured in Dulbecco's modified Eagle medium (DMEM) (Gibco, Grand Island, NY, USA) containing 10% fetal bovine serum (FBS). 4T1

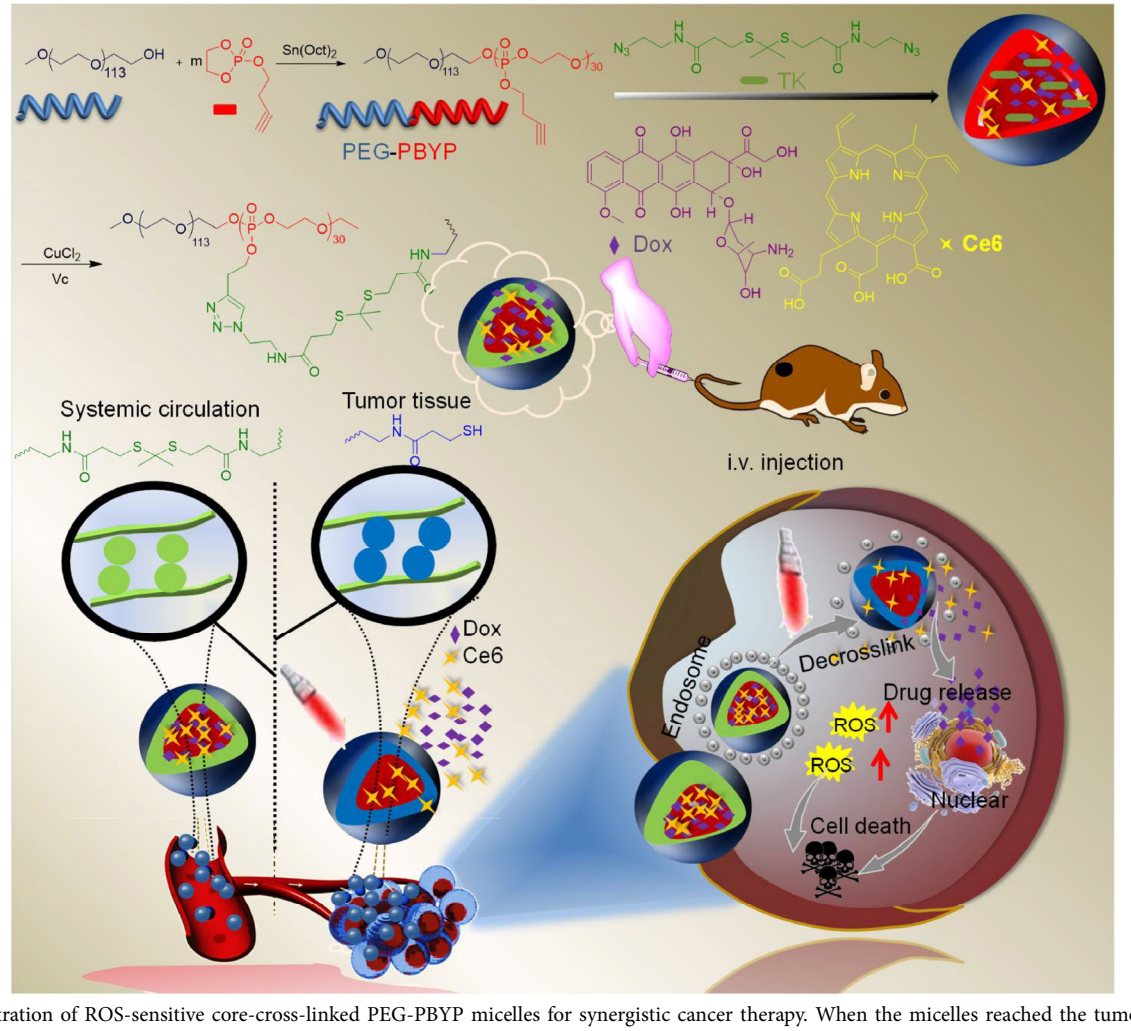

Scheme 1 Illustration of ROS-sensitive core-cross-linked PEG-PBYP micelles for synergistic cancer therapy. When the micelles reached the tumor areas through EPR effect and then entered the cells via endocytosis, the PS was activated to produce numerous of ROS, triggered decrosslinked of the micelles and speeded drug release.

cells were cultured in 1640 medium (Gibco, Grand Island, NY, USA) containing 10% FBS.

Female BALB/c mice (6–8 week, 18–20 g) were obtained from Shanghai Slaccas Experimental Animal Co., Ltd (Shanghai, China), and were housed in an SPF room. The animal experimental protocols were approved by the Institutional Animal Care and Use Committee, Soochow University.

2.2 Synthesis and characterization of poly(ethylene glycol)-block-poly(2-(but-3-yn-1-yloxy)-2-oxo-1,3,2-dioxaphospholane) (PEG-PBYP)

PEG-PBYP was synthesized via ring-opening polymerization (ROP) of BYP as initiated by PEG-OH [42]. Briefly, in a glovebox, BYP (105 mg, 0.6 mmol), $Sn(Oct)_2$ (8.1 mg, 0.02 mmol), and PEG-OH (100 mg, 0.02 mmol) were dissolved in anhydrous THF (5 mL), and the solution was stirred at 40 °C for 24 h. The final product PEG-PBYP was obtained as white powder after precipitation with diethyl ether/methanol (10:1, v/v). The copolymer structure was characterized by ^{1}H NMR, and the molecular weight distribution was determined by gel permeation chromatography (GPC) (Table S1 in the Electronic Supplementary Material (ESM)).

2.3 Synthesis and characterization of the TK-containing cross-linker

3-Mercaptopropionic acid (5.2 g, 49.1 mmol) and anhydrous acetone (5.8 g, 98.2 mmol) were mixed in a flask under a dry HCl atmosphere at room temperature. After 6 h, the mixture was crystallized in an ice-salt bath. The crude product was successively washed with hexane (3 × 50 mL) and cold water (3 × 50 mL), and 3,3'-(propane-2,2-diylbis(sulfanediyl))dipropionic acid (compound 1) was obtained as white solid (5.5 g, yield 65.2%) [43].

Sodium azide (5.85 g, 90 mmol) and 2-chloroethylamine hydrochloride (5.22 g, 45 mmol) were dissolved in water (50 mL), and the mixture was stirred at 80 °C for 24 h. After the pH was adjusted to 12 using NaOH solution (1 mol/L), the reaction mixture was extracted with Et_2O (3 × 50 mL). The organic phase was combined and dried over anhydrous Na_2SO_4. The mixture was filtered and the solvent was removed by vacuum. To avoid explosion, a small portion of solvent must be left. 3-Azidoethan-1-amine (compound 2) (7.5 g, yield 66.7%) was obtained as colorless oil [44].

Compound 1 (1.05 g, 1 mmol) and compound 2 (8.04 g, 2 mmol) were dissolved in dry DMF (30 mL). HBTU (606 mg, 1.6 mmol, 1.6 eq.) and HOBt (216 mg, 1.6 mmol, 1.6 eq.) dissolved in DMF (10 mL) were added. After stirring at room temperature for 24 h, the reaction mixture was extracted with Et_2O (3 × 100 mL). The organic phase was combined and dried over anhydrous Na_2SO_4 before the solvent was removed by vacuum. The crude product was purified by flash silica gel column chromatography with DCM/hexane (1/1, v/v) as the eluent, and the TK-containing cross-linker (compound 3) was obtained as yellow powder [45].

The non-responsive cross-linker, 1,6-diazidohexane (compound 4), was synthesized using a similar method as described before [46].

2.4 Preparation and characterization of micelles

The ROS-responsive core-cross-linked (RCCL) micelles, non-responsive core-cross-linked (NCCL) micelles, and un-cross-linked (UCL) micelles were prepared via the nanoprecipitation method (Table 1). Taking RCCL micelles as an example, PEG-PBYP (10 mg/mL in DMF, 100 μL, 1 eq. of alkyne groups) and compound 3 (10 mg/mL in DMF, 50 μL) were mixed together, which was added dropwisely into deionized water (2 mL) under vigorous stirring. After 1 h, $CuSO_4$ (4.1×10^{-3} mmol, 0.25 mol eq. of the alkynyl groups), sodium ascorbate (4.1×10^{-3} mmol, 0.25 mol eq. of the alkynyl groups) and PMDEM (4.1×10^{-3} μmol, 0.025 μmol eq. of the alkynyl groups) were added under the nitrogen atmosphere. After stirring for 24 h, the RCCL micelles were obtained followed by dialysis against deionized water for 24 h (MWCO = 3.5 kDa). The micelles were characterized by dynamic laser scattering (DLS) and transmission electron microscopy (TEM). Compound 4 instead of compound 3 was used to prepare the NCCL micelles using the same method. For UCL micelles, PEG-PBYP was nanoprecipitated into deionized water in the absence of the crosslinker using the similar method.

Pyrene was used as the probe to determine the critical micelle concentration (CMC) of the polymers [47]. Pyrene dissolved in acetone (0.6 mM, 1 mL) was put in the vial, and acetone was removed via volatilization. Then UCL micelles with different concentrations varied from 6.0×10^{-4} to 0.15 mM were added to the vials under stirring. The fluorescence intensity of the solution was recorded using a fluorescence spectrometer with the excitation wavelength of 290–360 nm and the emission wavelength of 390 nm. The cross-point of the intensity ratio I_{372}/I_{383} at the lowest and the highest concentration was the CMC of micelles.

2.5 Stability and ROS-triggered de-crosslinking of RCCL micelles

Sizes of the RCCL, NCCL, and UCL micelles (1 mg/mL in water) after dilution with DMF for 10 fold were determined by DLS. To probe the ROS-sensitivity, RCCL, NCCL, and UCL micelles (1 mg/mL in water) were treated with H_2O_2 (0.5 mM) for 4 h. Changes of the size and morphology were explored by DLS and TEM. The CMC of the TK-crosslinked PEG-PBYP after treatment with H_2O_2 (0.5 mM, 4 h) was also determined with the same method as described above.

2.6 Drug encapsulation and ROS-responsive drug release

The drug-loaded micelles were prepared using the same method as described for the blank micelles, except that the drug cargoes were mixed with the polymer and crosslinker before being nanoprecipitated into water. For example, in order to prepare Dox and Ce6-co-loaded RCCL micelles (RCCL-DC), PEG-PBYP (10 mg/mL in DMF, 100 μL, 1 eq. of the alkyne groups), compound 3 (10 mg/mL in DMF, 50 μL), Dox (5 mg/mL in DMF, 60 μL), and Ce6 (5 mg/mL in DMF, 60 μL) were mixed together and the solution was added dropwisely into deionized water (3 mL) (theoretical drug loading of both Dox and Ce6 at 23.1%) under vigorous stirring. After 1 h, $CuSO_4$ (4.1×10^{-3} mmol, 0.25 eq. of the alkyne groups), sodium ascorbate (4.1×10^{-3} mmol, 0.25 eq. of the alkyne groups), and PMDEM (4.1×10^{-3} μmol, 0.025 eq. of the alkyne groups) were added into the solution under nitrogen atmosphere. After 24 h, the micelles were obtained and dialyzed against deionized water for 24 h (MWCO = 3.5 kDa). The whole process was kept in the dark.

The Dox-loaded RCCL micelles (RCCL-Dox), Ce6-loaded RCCL micelles (RCCL-Ce6), and 1,1-dioctadecyl-3,3,3,3-tetramethylindotricarbocyanine iodide (DiR)-loaded RCCL micelles (RCCL-DiR) were prepared similarly. The Dox-loaded NCCL micelles (NCCL-Dox), Ce6-loaded NCCL micelles (NCCL-Ce6), and Dox- and Ce6-co-loaded NCCL micelles (NCCL-DC) were prepared similarly expect that the TK-containing cross-linker was replaced by the non-responsive cross-linker (compound 4).

The Dox- and Ce6-co-loaded un-cross-linked micelles (UCL-DC) were prepared as follows. PEG-PBYP (10 mg/mL in DMF, 100 μL), Dox (5 mg/mL in DMF, 60 μL), and Ce6 (5 mg/mL in DMF, 60 μL) were mixed together and the solution was added dropwisely into deionized water (3 mL) under vigorous stirring. After 4 h, the micelles were obtained and dialyzed against deionized water for 24 h (MWCO = 3.5 kDa). The whole process was kept in the dark. The DiR-loaded UCL micelles (UCL-DiR) were prepared using the same process.

To determine the drug loading in the micelles, RCCL-DC micelles (1 mL) were incubated with H_2O_2 (0.5 mM) for 4 h. Then, the mixture was taken (10 μL), mixed with DMF (990 μL), and kept in

the dark for 24 h. The content of Dox and Ce6 in the solution was determined by spectrofluorimetry (Dox: λ_{ex} = 485 nm, λ_{em} = 592 nm, Ce6: λ_{ex} = 630 nm, λ_{em} = 666 nm). Drug loading capacity (DLC) and drug loading efficiency (DLE) were calculated according to the following formulas

DLC (%) = (weight of loaded drug/total weight of polymer and loaded drug) × 100%
DLE (%) = (weight of loaded drug/weight of feeding drug) × 100%

To explore the ROS-responsive Dox release profiles, RCCL-Dox micelles (25 μg Dox/mL and 12.4 μg Ce6/mL, 1 mL) were placed in a dialysis bag (MWCO = 3.5 kDa) which was immersed in phosphate buffer saline (PBS) (7.4, 25 mL) containing H_2O_2 at various concentrations (0, 0.1, and 0.5 mM) and incubated at 37 °C under shaking. At determined time intervals, 2 mL of the release medium was withdrawn and refreshed with the same volume of release medium. The amount of Dox in the harvested release medium was determined by spectrofluorimetry (λ_{ex} = 485 nm, λ_{em} = 592 nm).

The light-triggered Dox release from RCCL-DC micelles was further explored. RCCL-DC micelles (25 μg Dox/mL and 12.4 μg Ce6/mL, 1 mL) were placed in a dialysis bag (MWCO = 3.5 kDa) and irradiated (660 nm, 5 mW/cm^2) for 0.5 h. The dialysis bag was then immersed in PBS (7.4, 25 mL) and incubated at 37 °C under shaking. The amount of Dox released at pre-determined time intervals was determined as described above.

2.7 Detection of light-mediated intracellular ROS production

Light-induced ROS generation in 4T1 cells was detected using a ROS probe, 2',7'-dichlorodihydrofluorescein diacetate (DCFH-DA). Cells were seeded in a 24-well plate at 3 × 10^4 cells/well and cultured for 24 h. RCCL-Ce6 micelles were added (1 μg Ce6/mL). After incubation for 4 h, the DCFH-DA solution was added (10 μM) and incubated with cells for another 20 min. The culture medium was replaced with fresh medium and irradiated (660 nm, 5 mW/cm^2) for 0.5 h. Cells were then fixed with paraformaldehyde (4%), stained with 4',6-diamidino-2-phenylindole (DAPI) (5 μg/mL), and observed by confocal laser scanning microscopy (CLSM).

2.8 *In vitro* cellular uptake

Briefly, 4T1 cells were seeded on 24-well plates (3 × 10^4 cells/well) and cultured for 24 h. The medium was replaced with fresh medium, into which UCL-DC, NCCL-DC, or RCCL-DC micelles were added at the final Dox concentration of 1 μg/mL and Ce6 concentration of 0.5 μg/mL. After incubation for 8 or 12 h, cells were fixed with 4% paraformaldehyde, stained with DAPI (5 μg/mL), and observed by CLSM. Alternatively, cells were treated with UCL-DC, RCCL-DC, and NCCL-DC micelles for 8 h, irradiated (660 nm, 5 mW/cm^2) for 0.5 h, and further incubated for 4 h before CLSM. To quantify the cellular uptake level, cells treated as described above were collected, resuspended in PBS, and subjected to flow cytometry analysis.

2.9 *In vitro* antitumor efficacy

The *in vitro* antitumor activity of the drug-loaded micelles was evaluated in 4T1 and MCF-7 cells. Briefly, cells were seeded in a 96-well plate at 7 × 10^3 cells/well and incubated for 24 h. The medium was replaced with fresh medium (90 μL), into which various micelles (RCCL-Dox, RCCL-Ce6, RCCL-DC, and NCCL-DC, 10 μL) were added at various final Dox equivalent concentrations. After incubation for 8 h, cells treated with RCCL-DC, RCCL-Ce6, and NCCL-DC micelles were irradiated (660 nm, 5 mW/cm^2) for 0.5 h. After incubation for another 48 h, the cell viability was determined using the MTT assay.

A live/dead double-staining assay was adopted to assess the cytotoxicity. 4T1 cells were seed on 24-well plates (3 × 10^4 cells/well), cultured for 24 h, treated with free Dox or various micelles at 2 μg Dox equivalent/mL for 8 h, irradiated (660 nm, 5 mW/cm^2) for 0.5 h, and further incubated for 48 h. Cells were then stained with calcein-acetoxymethyl ester (calcein-AM) (2 μM, for live cells) and propidium iodide (PI, 4.5 μM, for dead cells) for 15 min before observation by CLSM.

The cell apoptosis induced by drug-loaded micelles was further evaluated. 4T1 cells were seed on 6-well plates (3 × 10^6 cells/well) and treated with Dox or various micelles as described above. Cells were collected, stained using the Annexin V-FITC/PI kit (Beyotime, Shanghai, China), and subjected to flow cytometry analysis.

2.10 Pharmacokinetics and biodistribution

RCCL-DiR micelles, UCL-DiR micelles, or free DiR were i.v. injected to female BALB/c mice at 5.0 mg DiR/kg. At predetermined time points, blood (50 μL) was collected from the orbit and mixed with Triton X-100 (1%, 600 μL). DiR in the blood was extracted with HCl (1% in isopropyl alcohol, 900 μL), and the DiR content was determined by spectrofluorimetry (λ_{ex} = 748 nm, λ_{em} = 780 nm). The half-life time ($t_{1/2}$) of the micelles was calculated according to the previously reported method [48].

For the biodistribution study, 4T1 cells (2.5 × 10^6) were s.c. injected into the right flank of female BALB/c mice. When the tumor reached ~ 200 mm^3, RCCL-DiR micelles, UCL-DiR micelles, and free DiR were i.v. injected at 5.0 mg DiR/kg. Live animal fluorescence imaging was performed at predetermined time intervals (4, 6, 12, and 24 h post-injection) using a Maestro living imaging system (Cambridge Research and Instrumentation, Inc.). In another parallel study, mice were sacrificed at 12 h post injection, and the major organs (heart, liver, spleen, lung, and kidney) as well as tumors were collected and imaged. The relative fluorescence intensity of DiR in each tissue was quantified (λ_{ex} = 748 nm, λ_{em} = 780 nm).

2.11 *In vivo* antitumor efficacy

4T1 xenograft tumor-bearing mice as described above were used to evaluate the *in vivo* anticancer efficacy of drug-loaded micelles. When the tumor volume reached 50–60 mm^3, mice were randomly divided into six groups (eight mice per group), and they were i.v. injected with PBS, free Dox, RCCL-Dox, RCCL-Ce6, RCCL-DC, and UCCL-DC micelles on day 1, 4, and 7. The Dox and Ce6 doses for micelles were 10 and 4 mg/kg, respectively, while the dose for free Dox was 5 mg/kg. For RCCL-Ce6, RCCL-DC, and UCCL-DC micelles, the tumor sites were irradiated (660 nm, 5 mW/cm^2) for 0.5 h at 12 h post injection. The tumor volume and body weight were measured every other day. The tumor volume was calculated according to the following formula: (V = length × width × width/2). Mice with tumors larger than 1,000 mm^3 should be euthanized according to the standard animal protocol. Thus, on day 16, mice were sacrificed, and major organs as well as tumors were harvested, fixed with 10% formalin, embedded in paraffin, and sectioned. The tissue sections were stained with hematoxylin and eosin (H&E) for histological evaluation. The tumor tissues were also embedded in optimal cutting temperature (OCT) compound, frozen, and cryo-sectioned. The tumor sections were stained using the One Step TUNEL Apoptosis Assay kit (Beyotime Biotechnology) to evaluate tumor cell apoptosis.

2.12 Statistical analysis

Statistical analysis was performed using Student's *t*-test. The differences between two groups were determined to be significant at $^*p < 0.05$ and very significant at $^{**}p < 0.01$ and $^{***}p < 0.001$.

3 Results and discussion

3.1 Synthesis and characterization of PEG-PBYP copolymers

The PEG-PBYP polymer was synthesized via the ring-opening polymerization of BYP using PEG-OH as the macro-initiator and

$Sn(Oct)_2$ as the catalyst (Scheme S1 in the ESM). The polyphosphoester was selected as the backbone owing to its biocompatibility, biodegradability, and amenability for post-functionalization [49]. ^1H NMR analysis confirmed the successful synthesis of PEG-PBYP (Fig. S1 in the ESM), and the degree of polymerization (DP) of PBYP was calculated to be 28 by comparing the peak intensities of the methylene protons of PEG (δ, 3.70 ppm) and the alkynyl protons of BYP (δ, 2.5 ppm). The molecular weight (MW) and polydispersity index (PDI) of the PEG-PBYP polymer were determined to be 11.3 kDa and 1.20 by GPC, respectively (Table S1 in the ESM). Both the ROS-responsive, TK-containing cross-linker and the non-responsive cross-linker were synthesized accordingly (Scheme S1 in the ESM), and their structures were confirmed by ^1H NMR (Figs. S2–S5 in the ESM).

3.2 Characterization and ROS-sensitivity of the RCCL micelles

The micelles were prepared using the nanoprecipitation method, and they were chemically cross-linked to form CCL micelles. Sizes of the UCL, RCCL and NCCL micelles were determined to be around 91.5, 64.2, and 63.5 nm by DLS, respectively, with a narrow distribution (Fig. 1(a)). The reduced diameter of micelles after cross-linking could be attributed to the chemical cross-linking of the hydrophobic segment that rendered the micelle cores more compact. TEM images revealed spherical structures of the micelles, and revealed a more compact core of CCL micelles than the UCL micelles, as evidenced by the darkness in TEM images (Fig. 1(d)). Upon dilution with DMF for 10 fold, UCL micelle showed no DLS signals, indicating complete dissolution and dissociation of the micelles (Fig. 1(b)). In comparison, sizes of the NCCL and RCCL micelles slightly increased, presumably owing to the swelling of micelle cores. These results confirmed the stability of CCL micelles in organic solvents due to the core cross-linking via covalent bonding. Additionally, the stability of the micelles in different media was evaluated over storage for one week. CCL micelles maintained constant diameters in water (H_2O), PBS, cell growth medium (1640 medium), and 10% FBS (Fig. S6 in the ESM). However, UCL micelles lacking a stable core-cross-linked structure showed significantly increased diameters that indicated aggregation (Fig. S6 in the ESM). After treatment with H_2O_2, the diameter of RCCL micelles increased to ~ 94 nm (Figs. 1(c) and 1(d)), indicating cleavage of the TK linker and loosening of the micelle core. As a control, NCCL and UCL micelles with no H_2O_2 responsiveness maintained constant diameters and unaltered morphologies (Figs. 1(c) and 1(d)). Furthermore, the similar CMC values of UCL micelles (11.8 μg/mL) and H_2O_2-treated RCCL micelles (11.2 μg/mL) confirmed the cleavage of TK linkers and de-cross-linking of the RCCL micelles (Figs. 1(e) and 1(f)).

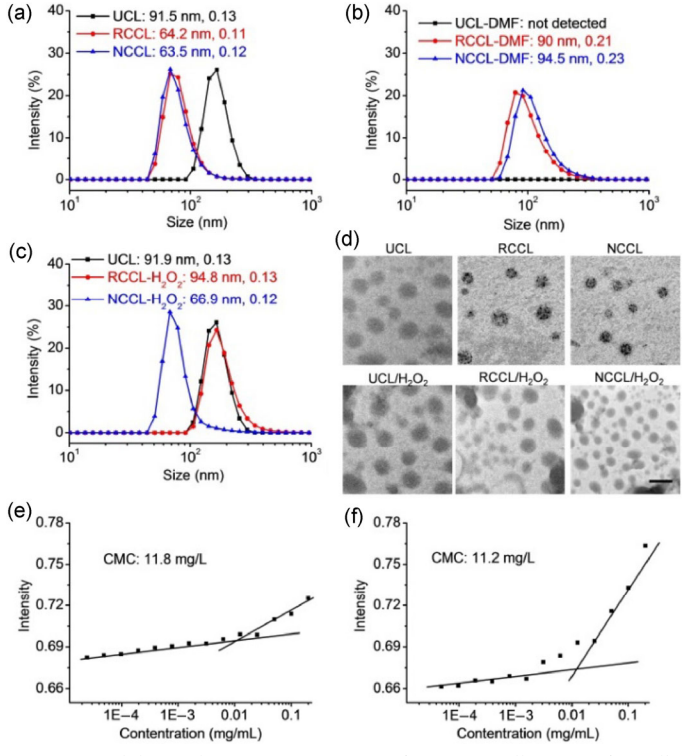

Figure 1 Stability and ROS responsiveness of RCCL micelles. Size of micelles in water (a), after dilution with DMF for 10 fold (b), and after treatment with 0.5 mM H_2O_2 (c). (d) TEM images of the micelles before and after H_2O_2 treatment (0.5 mM). CMC values of untreated UCL micelles (e) and RCCL micelles treated with 0.5 mM H_2O_2 (f).

3.3 Drug loading and *in vitro* release

PEG-PBYP polymers could self-assemble into micelles and encapsulate Dox and Ce6 in the cores via hydrophobic interactions. Drug-loaded UCL micelles (UCL-DC) showed large diameter of 171.2 nm with a wide distribution (Fig. 2(a)). In comparison, the cross-linked RCCL-DC micelles possessed notably smaller diameter of 84.5 nm, as confirmed by DLS analysis and TEM observation (Figs. 2(a) and 2(b)). DLC of Dox and Ce6 in the UCL-DC micelles was relatively low (4.1% and 0.9% for Dox and Ce6, respectively), while remarkably higher DLC was noted for the CCL micelles (12% and 4%–5% for Dox and Ce6, respectively), 3–5 fold higher than the ULC micelles (Table 2). It therefore demonstrated that the core cross-linking would benefit the drug encapsulation due to formation of a more compact hydrophobic core. When both Dox and Ce6 were encapsulated in the micelles, the DLE was slightly lower than that for the single drug-loaded micelles (Table 2). This may be due to the electrostatic repulsion between the polymer backbones and the Ce6 molecules that impeded successful encapsulation into the hydrophobic core.

The drug release from micelles was explored to verify the stability and responsiveness of the RCCL micelles both in the absence and presence of H_2O_2 (0.1 and 0.5 mM), a representative category of ROS. The RCCL-Dox micelles exhibited an H_2O_2 concentration-dependent drug release profile. In the absence of H_2O_2, the drug release from the RCCL-Dox micelles was quite slow with the cumulative release amount of ~ 30% within 36 h. In the presence of

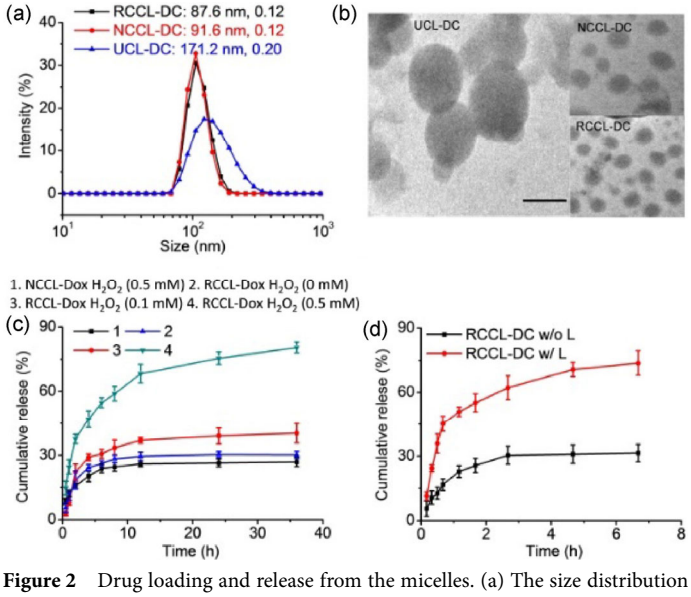

Figure 2 Drug loading and release from the micelles. (a) The size distribution of UCL-DC, RCCL-DC, and NCCL-DC micelles as measured by DLS. (b) Representative TEM images of the drug-loaded micelles. (c) Cumulative Dox release from NCCL-Dox and RCCL-Dox micelles in the presence and absence of H_2O_2 (n = 3). (d) Cumulative Dox release from RCCL-DC micelles with or without 0.5-h light irradiation (660 nm, 5 mW/cm^2) (n = 3).

Table 1 Abbreviations of micelles

Abbreviation	Full name
UCL	Un-cross-linked micelles
CCL	Core-cross-linked micelles
RCCL	ROS-responsive core-cross-linked micelles
NCCL	Non-responsive core-cross-linked micelles
RCCL-Dox	Dox-loaded RCCL micelles
RCCL-Ce6	Ce6-loaded RCCL micelles
RCCL-DC	Dox- and Ce6-co-loaded RCCL micelles
RCCL-DiR	DiR-loaded RCCL micelles
UCL-DC	Dox- and Ce6-co-loaded UCL micelles
UCL-DiR	DiR-loaded UCL micelles
NCCL-Dox	Dox-loaded NCCL micelles
NCCL-Ce6	Ce6-loaded UCCL micelles
NCCL-DC	Dox- and Ce6-co-loaded NCCL micelles

Table 2 Characterization of drug-loaded micelles

Micelle	Dox		Ce6	
	DLE (%)	DLC (%)	DLE (%)	DLC (%)
RCCL-Dox	89.6	15.2	—	—
RCCL-Ce6	—	—	32.5	6.1
RCCL-DC	84.9	12.4	30.5	4.9
NCCL-DC	84.2	12.3	25.6	4.0
UCL-DC	14.3	4.1	3.3	0.9

0.1 mM H_2O_2 (intracellular concentration in cancer cells) [24], drug release was slightly accelerated, indicating that the intracellular ROS was unable to efficiently trigger the de-crosslinking of micelles and drug release (Fig. 2(c)). Comparatively, at elevated H_2O_2 concentration (0.5 mM), pronounced drug release was noted, conferring a cumulative release amount of 80% within 36 h. As a non-responsive analogue, NCCL-Dox micelles showed unaltered release profile in the presence of 0.5 mM H_2O_2. Such observation therefore suggested the feasibility to enhance ROS concentration in cancer cells using PDT and accordingly accelerate drug release in response to ROS. In support of such hypothesis, more than 80% of the loaded Dox was released from RCCL-DC micelles within 4 h after light irradiation (Fig. 2(d)), indicating that the loaded PS can efficiently produce ROS to break down the TK cross-linker and promote micelle destabilization. Taken together, the introduction of TK cross-linker could not only increase the stability and the drug loading of the micelles, but also provide the micelles with the possibility of on-demand and instantaneous drug release upon external light triggers.

3.4 Intracellular ROS production

The light-induced ROS production in 4T1 cells was probed using a ROS probe, DCFH-DA. The non-fluorescent DCFH-DA can be oxidized to fluorescent dichlorofluorescein (DCF) by cellular ROS. After 0.5-h light irradiation (660 nm, 5 mW/cm^2), the DCF fluorescence (green) in cells treated with RCCL-Ce6 micelles enhanced significantly, demonstrating sufficient ROS production. However, cells treated with PBS or RCCL-Ce6 micelles without light activation exhibited weak fluorescence signal (Fig. S7 in the ESM). Addition of Vc, an antioxidant to deplete ROS, to the cells before light irradiation could remarkably attenuate the DCF fluorescence intensity in the cells. The results substantiated the enhanced intracellular ROS level induced by light activation of Ce6.

3.5 *In vitro* cellular uptake

The cellular uptake and intracellular distribution of micelles were evaluated in 4T1 cells by CLSM and flow cytometry. As shown in Fig. 3(a), more red fluorescence signal was detected in the cells treated with UCL-Dox micelles than those treated with RCCL-Dox or NCCL-Dox micelles for either 8 or 12 h (Figs. 3(a) and 3(b)). The same trend was observed for the flow cytometry analysis and the quantified fluorescence intensity (Figs. 3(e)–3(g)). Such discrepancy was probably because UCL-Dox micelles released Dox faster than the CCL micelles, and the fluorescence of the encapsulated Dox in the micelles core could be partially quenched [48]. Nevertheless, when light irradiation (606 nm, 5 mW/cm^2, 0.5 h) was performed at 8 h post incubation with micelles followed by incubation for another 4 h, the RCCL-DC micelles exhibited comparable intracellular fluorescence intensity to the UCL micelles, notably outperforming the NCCL-DC micelles (Figs. 3(c), 3(h), and 3(i)), These results thus suggested the efficient drug release from RCCL-DC micelles upon light-induced ROS generation.

3.6 *In vitro* anti-cancer efficacy

The cytotoxicity of the blank micelles was first investigated using the MTT assay. The viability of both 4T1 and MCF-7 cells remained above 90% after incubation with micelles at the concentration range from 1 to 500 μg/mL, indicating low toxicity of the drug carrier (Fig. S8 in the ESM). Then the anti-cancer efficacy of the drug-loaded micelles was evaluated using the same cell lines. As shown in Figs. 4(a) and 4(b), RCCL-DC micelles exhibited significantly stronger

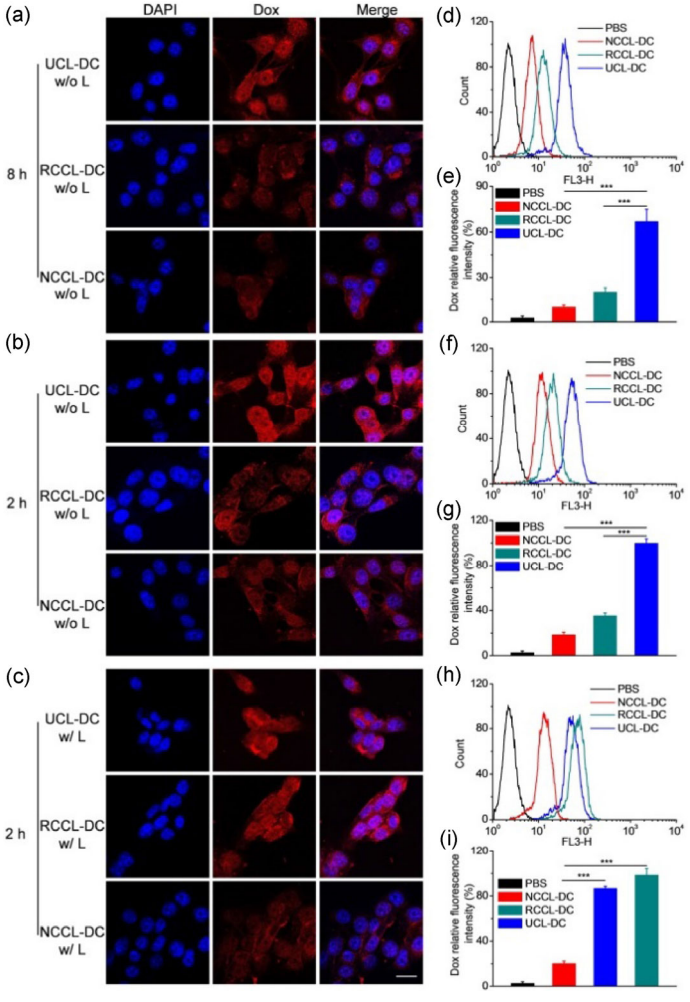

Figure 3 Cellular uptake and intracellular distribution of micelles. (a)–(c) Representative CLSM images of 4T1 cells following incubation with different micelles for 8 or 12 h. Scale bar = 50 μm. Flow cytometry analysis of the intracellular Dox content after treatment with different micelles for 8 h (d) and (e), 12 h without irradiation (f) and (g), and 12 h with irradiation (h) and (i). Light irradiation (660 nm, 5 mW/cm^2, 0.5 h) was performed after 8-h incubation with micelles (n = 3).

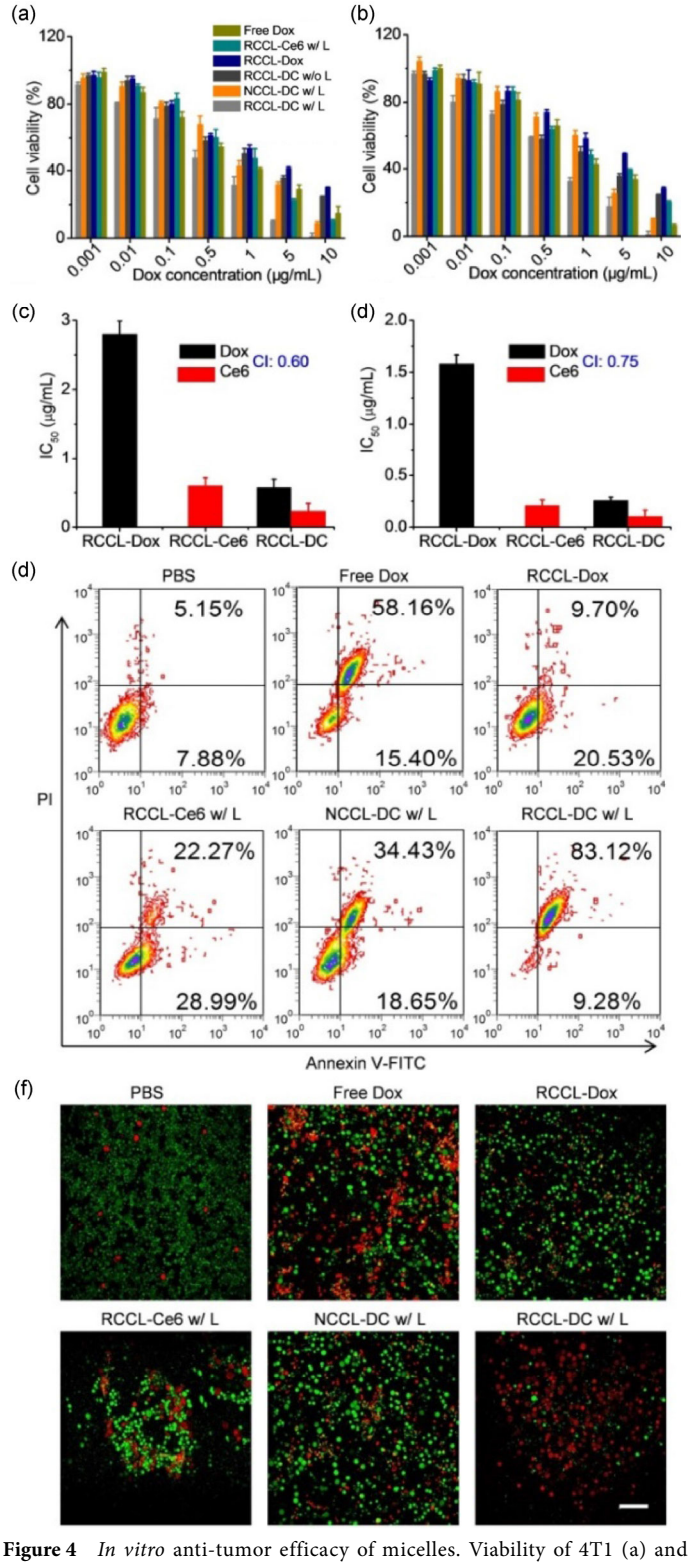

Figure 4 *In vitro* anti-tumor efficacy of micelles. Viability of 4T1 (a) and MCF-7 (b) cells after treatment with different micelles. IC_{50} of Dox and Ce6 in 4T1 (c) and MCF-7 (d) cells after treatment with different micelles. (e) Flow cytometric analysis of 4T1 cells treated with different micelles and stained with Annexin V-FITC/PI. (f) CLSM images of 4T1 cells treated with different micelles and double-stained with calcein-AM (green, live cells) and PI (red, dead cells). Scale bar = 100 μm. For all the experiments, cells were incubated with micelles for 8 h, irradiated (660 nm, 5 mW/cm^2) for 0.5 h, and incubated for an additional 48 h before the assessments.

anticancer efficacy than RCCL-Dox micelles (Dox only), RCCL-Ce6 micelles (Ce6 only), and NCCL-DC micelles (non-responsive) after 30-min light irradiation. The half-maximal inhibitory concentration (IC_{50}) of Dox in RCCL-DC micelles (0.62 μg/mL for 4T1 cells and 0.42 μg/mL for MCF-7 cells) was 3–4-fold lower than that in RCCL-Dox micelles (2.8 μg/mL for 4T1 cells and 1.6 μg/mL for MCF-7 cells). The combination index (CI) between Dox and Ce6 in RCCL-DC micelles was far below 1 (0.60 in 4T1 cells and 0.75 in MCF-7 cells) (Figs. 4(c) and 4(d)), substantiating the synergistic effect between Dox and Ce6 as a result of the light activated, PS-mediated ROS generation and subsequent ROS-triggered fast Dox release in cancer cells [50].

Additionally, the potency of the drug-loaded micelles to induce cancer cell apoptosis was measured using the Annexin V-FITC/PI assay. As shown in Fig. 4(e), the apoptosis rates induced by RCCL-Dox, RCCL-Ce6, and NCCL-DC micelles were 30.23%, 51.26%, and 53.08%, respectively. In contrast, RCCL-DC micelles induced significantly augmented apoptosis rate of 92.40%, which accorded well with their anti-cancer efficacy as demonstrated by the MTT assay (Fig. 4(a)).

CLSM images were used to visualize both the dead and live cells after treatments, using the calcein-AM and PI double staining assay (Fig. 4(f)). Live cells enzymatically hydrolyze the non-fluorescent calcein-AM to the green fluorescent calcein, while the PI molecule can penetrate the cell membrane of dead cells and bind to DNA to emit red fluorescence [51]. Compared with cells treated with RCCL-Dox, RCCL-Ce6, and NCCL-DC micelles, cells treated with RCCL-DC micelles showed the highest density of red fluorescence, indicating their strongest cancer cell killing efficiency (Fig. 4(f)).

3.7 Pharmacokinetics and biodistribution

As shown in Fig. 5(a), RCCL-DiR micelles exhibited prolonged blood circulation time than free DiR and UCL-DiR micelles after i.v. injection, and the half-life ($t_{1/2}$) of the RCCL-DiR micelles was 5.3 h, 2.1- and 10.6-fold longer than UCL-DiR micelles (2.5 h) and free DiR (0.5 h), respectively. Such prolonged blood circulation time of RCCL micelles may be attributed to the stealth property of the PEG shells and the stable core-cross-linked structures of the CCL micelles that prevented dissociation and pre-leakage of the drug cargoes upon extensive dilution by the blood. The biodistribution of micelles was further assessed in 4T1 xenograft tumor-bearing mice. As shown in Fig. 5(b), RCCL-DiR micelles showed notably stronger fluorescence

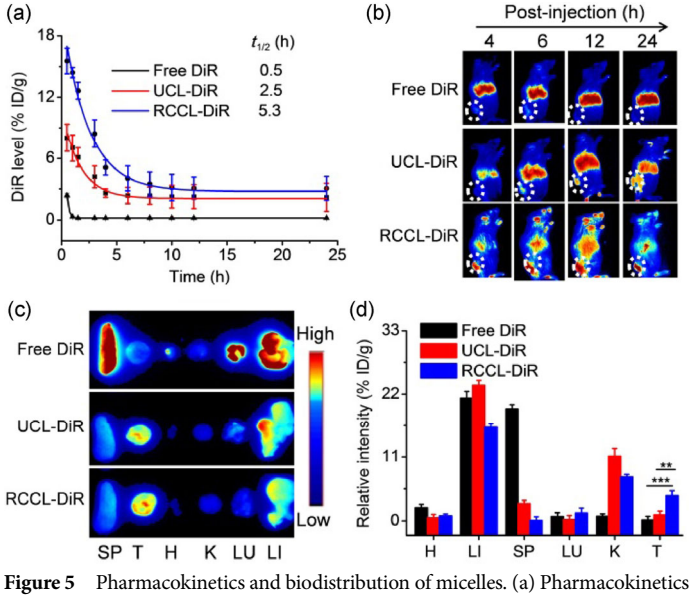

Figure 5 Pharmacokinetics and biodistribution of micelles. (a) Pharmacokinetics of RCCL-DiR micelles, UCL-DiR micelles, and free DiR following i.v. injection (n = 3). (b) Fluorescence imaging of 4T1 tumor-bearing mice at different time post i.v. injection of RCCL-DiR micelles, UCL-DiR micelles, and free DiR. (c) *Ex vivo* fluorescence imaging of excised tumors and major organs at 12 h post i.v. injection (H: heart; LI: liver; SP: spleen; LU: lung; K: kidney; T: tumor). (d) Biodistribution levels of DiR in tumors and major organs at 12 h post i.v. injection (n = 3).

intensity of DiR in the tumors than free DiR and UCL-DiR micelles, and the fluorescence intensity peaked at 12 h post injection. After injection, most of the free DiR was accumulated and trapped in livers, and UCL-DiR micelles also showed a progressive accumulation in livers owing to the undesired stability of the micelles (Fig. 5(b)). Notably, the RCCL micelles showed pronounced passive targeting to tumor sites mainly ascribed to the prolonged systemic circulation and the EPR effect. Then, the major organs and tumors were harvested at 12 h post injection, and the *ex vivo* fluorescence intensity further quantified (Figs. 5(c) and 5(d)). The DiR content in the tumors treated with RCCL-DiR micelles was 8- and 2-fold higher than those of DiR- and UCL-DiR micelles-treated tumors, respectively. Taken together, these findings demonstrated the advantage of the RCCL micelles with chemically-stabilized structure to enable prolonged blood circulation and enhanced tumor accumulation following i.v. injection.

3.8 *In vivo* antitumor efficacy

A 4T1 xenograft tumor-bearing murine model was used to evaluate the anticancer efficacy of the micelles. The mice were i.v. injected with PBS, free Dox (5 mg/kg), RCCL-Dox (10 mg Dox/kg), RCCL-Ce6 (4 mg Ce6/kg), NCCL-DC (10 mg Dox/kg, 4 mg Ce6/kg), and RCCL-DC (10 mg Dox/kg, 4 mg Ce6/kg). Free Dox was injected at 5 mg/kg due to its serious heart toxicity [50]. Based on the biodistribution results, 30-min light irradiation was applied at 12 h post injection. As indicated in Figs. 6(a) and 6(b), the tumors after treatment with PBS grew rapidly and reached the size around 1,200 mm^3 within 16 days. Free Dox and RCCL-Dox showed similar and weak tumor inhibition efficacy. RCCL-Ce6 and NCCL-DC micelles showed a stronger inhibition rate of tumor growth compared to free Dox, which could be due to the photodynamic effect of the encapsulated Ce6. Importantly, the RCCL-DC micelles, upon light activation, completely suppressed the growth of solid tumors within the 16-day observation period. Among all the treatments, free Dox showed remarkable side effect as evidenced by a ~ 10% reduction of the body weight (Fig. 6(c)), while negligible body weight loss was noted for all test micelles. In accordance with the tumor inhibition capability, the RCCL-DC micelles significantly enhanced the survival rate of the tumor-bearing mice over the 40-day observation period (Fig. 6(d)). Additionally, tumors treated with RCCL-DC micelles exhibited the highest tumor cell remission rate in H&E-stained tumor tissues (Fig. 6(e)) and the highest tumor cell apoptosis rate after TUNEL staining (Fig. 6(f)). Histological observation on major organs revealed lack of pathological abnormalities following treatment with RCCL-DC micelles (Fig. S9 in the ESM). These results collectively demonstrated the effective and synergistic anti-cancer effect of the RCCL micelles, which would undergo ROS-induced destabilization upon light irradiation to accelerate Dox release and thereby enabling potent and synergistic anti-cancer efficacy with negligible side toxicity to normal tissues.

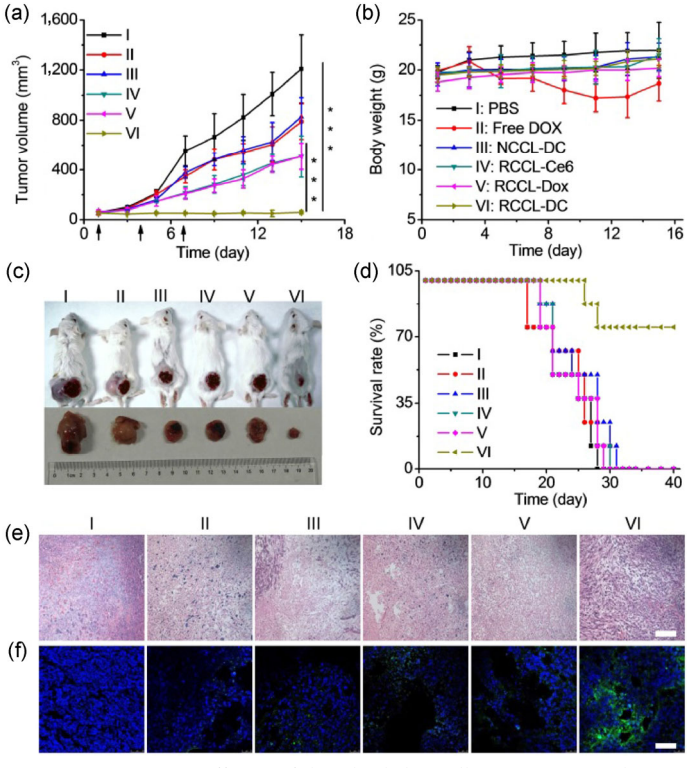

Figure 6 Anti-tumor efficacy of drug-loaded micelles in 4T1 tumor-bearing mice. Tumor volume (a) and body weight (b) of mice during the 16-day observation period. (c) Representative images of tumors on day 16 (b). (d) Survival rate of mice within the 40-day observation period. (e) H&E-stained tumor tissues on day 16. Scale bar = 100 μm. (f) Cell apoptosis in tumor tissues harvested on day 16 as determined by TUNEL staining. Scale bar = 100 μm. Mice were i.v. injected with PBS, free Dox, RCCL-Dox micelles, RCCL-Ce6 micelles, NCC-DC micelles, and RCCL-DC micelles on day 1, 4 and 7 (4 mg Ce6/kg and 10 mg Dox,/kg for micelles, 5 mg/kg for free Dox) (n = 8). Tumor sites were irradiated (660 nm, 5 mW/cm^2) for 0.5 h at 12 h post injection of micelles.

4 Conclusions

In summary, we developed a ROS-responsive CCL micellar system to enhance the circulation stability and allow on-demand chemodrug release via PS-induced ROS generation upon far red light irradiation. The RCCL micelles were core-cross-linked via a TK-containing linker, which efficiently stabilized the micelles, enhanced the loading capacity for Dox and Ce6, and prevented the pre-leakage of drug cargoes upon dilution. In the tumor tissues, the loaded Ce6 in RCCL-DC micelles produced extensive ROS under light activation to cleave the TK linkers and disrupt the micelle cores. As such, micelles were destabilized to accelerate Dox release, thereby provoking synergistic anti-cancer effect with ROS-mediated photodynamic therapy. This study provides an effective strategy to resolve the dilemma of formulation stability and effective as well as cancer-selective drug release, and would thus render a promising modality for the anti-cancer combination therapy.

Acknowledgements

This work was supported by the National Natural Science Foundation of China (Nos. 51722305, 51573123, and 51873142), the Ministry of Science and Technology of China (No. 2016YFA0201200), the 111 Project, and Priority Academic Program Development of Jiangsu Higher Education Institutions (PAPD).

Electronic Supplementary Material: Supplementary material (the synthetic routes of PEG-PBYP, ^{1}H NMR spectra, size variations of micelles, cytotoxicity, tissue histology, etc.) is available in the online version of this article at https://doi.org/10.1007/s12274-019-2330-y.

References

[1] Wicki, A.; Witzigmann, D.; Balasubramanian, V.; Huwyler, J. Nanomedicine in cancer therapy: Challenges, opportunities, and clinical applications. *J. Control. Release* **2015**, *200*, 138–157.

[2] Kwon, G. S.; Okano, T. Polymeric micelles as new drug carriers. *Adv. Drug Deliv. Rev.* **1996**, *21*, 107–116.

[3] Kataoka, K.; Harada, A.; Nagasaki, Y. Block copolymer micelles for drug delivery: Design, characterization and biological significance. *Adv. Drug Deliv. Rev.* **2012**, *64*, 37–48.

[4] Duncan, R. The dawning era of polymer therapeutics. *Nat. Rev. Drug Dis.* **2003**, *2*, 347–360.

[5] Aouameur, D.; Cheng, H.; Opoku-Damoah, Y.; Sun, B.; Dong, Q. L.; Han, Y.; Zhou, J. P.; Ding, Y. Stimuli-responsive gel-micelles with flexible modulation of drug release for maximized antitumor efficacy. *Nano Res.* **2018**, *11*, 4245–4264.

[6] Stuart, M. A. C.; Huck, W. T. S.; Genzer, J.; Müller, M.; Ober, C.; Stamm, M.; Sukhorukov, G. B.; Szleifer, I.; Tsukruk, V. V.; Urban, M. et al. Emerging applications of stimuli-responsive polymer materials. *Nat. Mater.* **2010**, *9*, 101–113.

[7] Cao, Z. Y.; Ma, Y. C.; Sun, C. Y.; Lu, Z. D.; Yao, Z. Y.; Wang, J. X.; Li, D. D.; Yuan, Y. Y.; Yang, X. Z. ROS-sensitive polymeric nanocarriers with red light-activated size shrinkage for remotely controlled drug release. *Chem. Mater.* **2017**, *30*, 517–525.

[8] Ding, D.; Zhu, Z. S.; Li, R. T.; Li, X. L.; Wu, W.; Jiang, X. Q.; Liu, B. R. Nanospheres-incorporated implantable hydrogel as a trans-tissue drug delivery system. *ACS Nano* **2011**, *5*, 2520–2534.

[9] Phelps, E. A.; Enemchukwu, N. O.; Fiore, V. F.; Sy, J. C.; Murthy, N.; Sulchek, T. A.; Barker, T. H.; García, A. J. Maleimide cross-linked bioactive peg hydrogel exhibits improved reaction kinetics and cross-linking for cell encapsulation and *in situ* delivery. *Adv. Mater.* **2012**, *24*, 64–70.

[10] Wang, P .; Wang, J. X.; Tan, H. W.; Weng, S. F.; Cheng, L. Y.; Zhou, Z. P.; Wen, S. Acid- and reduction-sensitive micelles for improving the drug delivery efficacy for pancreatic cancer therapy. *Biomater. Sci.* **2018**, *6*, 1262–1270.

[11] Shuai, X. T.; Merdan, T.; Schaper, A. K.; Xi, F.; Kissel, T. Core-cross-linked polymeric micelles as paclitaxel carriers. *Bioconjugate Chem.* **2004**, *15*, 441–448.

[12] Talelli, M.; Barz, M.; Rijcken, C. J. F.; Kiessling, F.; Hennink, W. E.; Lammers, T. Core-crosslinked polymeric micelles: Principles, preparation, biomedical applications and clinical translation. *Nano Today* **2015**, *10*, 93–117.

[13] Li, Y. P.; Xiao, K.; Luo, J. T.; Xiao, W. W.; Lee, J. S.; Gonik, A. M.; Kato, J.; Dong, T. A.; Lam, K. S. Well-defined, reversible disulfide cross-linked micelles for on-demand paclitaxel delivery. *Biomaterials* **2011**, *32*, 6633–6645.

[14] Gulfam, M.; Matini, T.; Monteiro, P. F.; Riva, R.; Collins, H.; Spriggs, K.; Howdle, S. M.; Jérôme, C.; Alexander, C. Bioreducible cross-linked core polymer micelles enhance *in vitro* activity of methotrexate in breast cancer cells. *Biomater. Sci.* **2017**, *5*, 532–550.

[15] Pitarresi, G.; Casadei, M. A.; Mandracchia, D.; Paolicelli, P.; Palumbo, F. S.; Giammona, G. Photocrosslinking of dextran and polyaspartamide derivatives: A combination suitable for colon-specific drug delivery. *J. Control. Release* **2007**, *119*, 328–338.

[16] Ding, J. X.; Zhuang, X. L.; Xiao, C. S.; Cheng, Y. L.; Zhao, L.; He, C. L.; Tang, Z. H.; Chen, X. S. Preparation of photo-cross-linked pH-responsive polypeptide nanogels as potential carriers for controlled drug delivery. *J. Mater. Chem.* **2011**, *21*, 11383–11391.

[17] Yang, S. C.; Tang, Z. H.; Zhang, D. W.; Deng, M. X.; Chen, X. S. pH and redox dual-sensitive polysaccharide nanoparticles for the efficient delivery of doxorubicin. *Biomater. Sci.* **2017**, *5*, 2169–2178.

[18] Li, J. M.; Liu, Y.; Li, H. L.; Shi, W.; Bi, X. Z.; Qiu, Q. Q.; Zhang, B.; Huang, W. L.; Qian, H. pH-sensitive micelles with mitochondria-targeted and aggregation-induced emission characterization: Synthesis, cytotoxicity and biological applications. *Biomater. Sci.* **2018**, *6*, 2998–3008.

[19] Li, X.; Li, H.; Yi, W.; Chen, J. Y.; Liang, B. L. Acid-triggered core cross-linked nanomicelles for targeted drug delivery and magnetic resonance imaging in liver cancer cells. *Int. J. Nanomedicine* **2013**, *8*, 3019–3031.

[20] Wang, X. R.; Liu, G. H.; Hu, J. M.; Zhang, G. Y.; Liu, S. Y. Concurrent block copolymer polymersome stabilization and bilayer permeabilization by stimuli-regulated "traceless" crosslinking. *Angew. Chem.* **2014**, *126*, 3202–3206.

[21] Zhang, Z. H.; Yin, L. C.; Tu, C. L.; Song, Z. Y.; Zhang, Y. F.; Xu, Y. X.; Tong, R.; Zhou, Q.; Ren, J.; Cheng, J. J. Redox-responsive, core cross-linked polyester micelles. *ACS Macro Lett.* **2013**, *2*, 40–44.

[22] Zhang, Y.; Guo, Q.; An, S.; Lu, Y. F.; Li, J. F.; He, X.; Liu, L. S.; Zhang, Y. J.; Sun, T.; Jiang, C. ROS-switchable polymeric nanoplatform with stimuli-responsive release for active targeted drug delivery to breast cancer. *ACS Appl. Mater. Interfaces* **2017**, *9*, 12227–12240.

[23] Hu, X. L.; Chen, X. S.; Wei, J. Z.; Liu, S.; Jing, X. B. Core crosslinking of biodegradable block copolymer micelles based on poly(ester carbonate). *Macromol. Biosci.* **2009**, *9*, 456–463.

[24] Li, J.; Sun, C. Y.; Tao, W.; Cao, Z. Y.; Qian, H. S.; Yang, X. Z.; Wang, J. Photoinduced PEG deshielding from ROS-sensitive linkage-bridged block copolymer-based nanocarriers for on-demand drug delivery. *Biomaterials* **2018**, *170*, 147–155.

[25] Ruan, C. H.; Liu, L. S.; Wang, Q. B.; Chen, X. L.; Chen, Q. J.; Lu, Y. F.; Zhang, Y.; He, X.; Zhang, Y. J.; Guo, Q. et al. Reactive oxygen species-biodegradable gene carrier for the targeting therapy of breast cancer. *ACS Appl. Mater. Interfaces* **2018**, *10*, 10398–10408.

[26] Kramer, J. R.; Deming, T. J. Glycopolypeptides with a redox-triggered helix-to-coil transition. *J. Am. Chem. Soc.* **2012**, *134*, 4112–4115.

[27] Han, P.; Li, S. C.; Cao, W.; Li, Y.; Sun, Z. W.; Wang, Z. Q.; Xu, H. P. Red light responsive diselenide-containing block copolymer micelles. *J. Mater. Chem. B* **2013**, *1*, 740–743.

[28] Liu, J. Y.; Pang, Y.; Zhu, Z. Y.; Wang, D. L.; Li, C. T.; Huang, W.; Zhu, X. Y.; Yan, D. Y. Therapeutic nanocarriers with hydrogen peroxide-triggered drug release for cancer treatment. *Biomacromolecules* **2013**, *14*, 1627–1636.

[29] Wang, L.; Fan, F. Q.; Cao, W.; Xu, H. P. Ultrasensitive ROS-responsive coassemblies of tellurium-containing molecules and phospholipids. *ACS Appl. Mater. Interfaces* **2015**, *7*, 16054–16060.

[30] Cao, W.; Gu, Y. W.; Li, T. Y.; Xu, H. P. Ultra-sensitive ROS-responsive tellurium-containing polymers. *Chem. Commun.* **2015**, *51*, 7069–7071.

[31] Wang, J. Q.; Zhang, Y. Q.; Archibong, E.; Ligler, F. S.; Gu, Z. Leveraging H_2O_2 levels for biomedical applications. *Adv. Biosyst.* **2017**, *1*, 1700084.

[32] Wang, C.; Wang, J. Q.; Zhang, X. D.; Yu, S. J.; Wen, D.; Hu, Q. Y.; Ye, Y. Q.; Bomba, H.; Hu, X. L.; Liu, Z. et al. *In situ* formed reactive oxygen species-responsive scaffold with gemcitabine and checkpoint inhibitor for combination therapy. *Sci. Transl. Med.* **2018**, *10*, eaan3682.

[33] Song, X. J.; Feng, L. Z.; Liang, C.; Gao, M.; Song, G. S.; Liu, Z. Liposomes co-loaded with metformin and chlorin e6 modulate tumor hypoxia during enhanced photodynamic therapy. *Nano Res.* **2017**, *10*, 1200–1212.

[34] Bhaumik, J.; Mittal, A. K.; Banerjee, J.; Chisti, Y.; Banerjee, U. C. Applications of phototheranostic nanoagents in photodynamic therapy. *Nano Res.* **2015**, *8*, 1373–1394.

[35] Dang, J. J.; He, H.; Chen, D. L.; Yin, L. C. Manipulating tumor hypoxia toward enhanced photodynamic therapy (PDT). *Biomater. Sci.* **2017**, *5*, 1500–1511.

[36] Dolmans, D. E. J. G. J.; Fukumura, D.; Jain, R. K. Photodynamic therapy for cancer. *Nat. Rev. Cancer* **2003**, *3*, 380–387.

[37] Sung, S. Y.; Su, Y. L.; Cheng, W.; Hu, P. F.; Chiang, C. S.; Chen, W. T.; Hu, S. H. Graphene quantum dots-mediated theranostic penetrative delivery of drug and photolytics in deep tumors by targeted biomimetic nanosponges. *Nano Lett.* **2018**, *19*, 69–81.

[38] Cui, S. S.; Yin, D. Y.; Chen, Y. Q.; Di, Y. F.; Chen, H. Y.; Ma, Y. X.; Achilefu, S.; Gu, Y. Q. *In vivo* targeted deep-tissue photodynamic therapy based on near-infrared light triggered upconversion nanoconstruct. *ACS Nano* **2013**, *7*, 676–688.

[39] Idris, N. M.; Gnanasammandhan, M. K.; Zhang, J.; Ho, P. C.; Mahendran, R.; Zhang, Y. *In vivo* photodynamic therapy using upconversion nanoparticles as remote-controlled nanotransducers. *Nat. Med.* **2012**, *18*, 1580–1585.

[40] Qin, W.; Ding, D.; Liu, J. Z.; Yuan, W. Z.; Hu, Y.; Liu, B.; Tang, B. Z. Biocompatible nanoparticles with aggregation-induced emission characteristics as far-red/near-infrared fluorescent bioprobes for *in vitro* and *in vivo* imaging applications. *Adv*. *Funct*. *Mater*. **2012**, *22*, 771–779.

[41] Du, X. Q.; Sun, Y.; Zhang, M. Z.; He, J. L.; Ni, P. H. Polyphosphoester-camptothecin prodrug with reduction-response prepared via michael addition polymerization and click reaction. *ACS Appl*. *Mater*. *Interfaces* **2017**, *9*, 13939–13949.

[42] Hu, J.; He, J. L.; Zhang, M. Z.; Ni, P. H. Folate-conjugated biodegradable core cross-linked polyphosphoester micelles for targeted and pH-triggered drug delivery. *J*. *Control*. *Release* **2015**, *213*, e86–e87.

[43] Yuan, Y. Y.; Liu, J.; Liu, B. Conjugated-polyelectrolyte-based polyprodrug: Targeted and image-guided photodynamic and chemotherapy with on-demand drug release upon irradiation with a single light source. *Angew*. *Chem*. **2014**, *126*, 7291–7296.

[44] Mock, W. L.; Irra, T. A.; Wepsiec, J. P.; Manimaran, T. L. Cycloaddition induced by cucurbituril. A case of Pauling principle catalysis. *J*. *Org*. *Chem*. **1983**, *48*, 3619–3620.

[45] He, Y. Y.; Cheng, G.; Xie, L.; Nie, Y.; He, B.; Gu, Z. W. Polyethyleneimine/DNA polyplexes with reduction-sensitive hyaluronic acid derivatives shielding for targeted gene delivery. *Biomaterials* **2013**, *34*, 1235–1245.

[46] Li, F. F.; Li, Y. J.; Zhou, Z. C.; Lv, S. X.; Deng, Q. R.; Xu, X.; Yin, L. C. Engineering the aromaticity of cationic helical polypeptides toward "self-activated" DNA/siRNA delivery. *ACS Appl*. *Mater*. *Interfaces* **2017**, *9*, 23586–23601.

[47] Lv, S. X.; Wu, Y. C.; Dang, J. Q.; Tang, Z. H.; Song, Z. Y.; Ma, S.; Wang, X.; Chen, X S.; Cheng, J. J.; Yin, L. C. Investigation on the controlled synthesis and post-modification of poly-[(N-2-hydroxyethyl)-aspartamide]-based polymers. *Polym*. *Chem*. **2017**, *8*, 1872–1877.

[48] Deepagan, V. G.; Kwon, S.; You, D. G.; Van Quy Nguyen; Um, W.; Ko, H.; Lee, H.; Jo, D. G.; Kang, Y. M.; Park, J. H. *In situ* diselenide-crosslinked polymeric micelles for ROS-mediated anticancer drug delivery. *Biomaterials* **2016**, *103*, 56–66.

[49] Zhao, Z.; Wang, J.; Mao, H. Q.; Leong, K. W. Polyphosphoesters in drug and gene delivery. *Adv*. *Drug Deliv*. *Rev*. **2003**, *55*, 483–499.

[50] Li, Y. J.; Lv, S. X.; Song, Z. Y.; Dang, J. J.; Li, X. D.; He, H.; Xu, X.; Zhou, Z. C.; Yin, L. C. Photodynamic therapy-mediated remote control of chemotherapy toward synergistic anticancer treatment. *Nanoscale* **2018**, *10*, 14554–14562

[51] Liu, Y.; Song, N.; Chen, L.; Xie, Z. G. Bodipy@ir(III) complexes assembling organic nanoparticles for enhanced photodynamic therapy. *Chin*. *J*. *Polym*. *Sci*. **2018**, *36*, 417–424.